Journal of Ginseng Research 45 (2021) 631–641

Contents lists available at ScienceDirect

Journal of Ginseng Research

journal homepage: https://www.sciencedirect.com/journal/journal-of-ginseng-research

Research Article

Whitening and inhibiting NF-κB-mediated inflammation properties of the biotransformed green ginseng berry of new cultivar K1, ginsenoside Rg2 enriched, on B16 and LPS-stimulated RAW 264.7 cells

Xing Yue Xu [a], Eun Seob Yi [a], Chang Ho Kang [b], Ying Liu [a], Yeong-Geun Lee [a], Han Sol Choi [a], Hyun Bin Jang [a], Yue Huo [a], Nam-In Baek [a], Deok Chun Yang [a], Yeon-Ju Kim [a, *]

[a] Graduate School of Biotechnology, and College of Life Science, Kyung Hee University, Yongin-si, Gyeonggi-do, Republic of Korea
[b] Division of Applied Life Science and PMBBRC, Gyeongsang National University, Jinju, Republic of Korea

ARTICLE INFO

Article history:
Received 8 July 2020
Received in revised form
18 February 2021
Accepted 19 February 2021
Available online 14 March 2021

Keywords:
Anti-inflammation
β-glucosidase (bgp1)
Ginsenosides
Ginseng cultivar K-1
Whitening

ABSTRACT

Background: Main bioactive constituents and pharmacological functions of ripened red ginseng berry (*Panax ginseng* Meyer) have been frequently reported. Yet, the research gap targeting the beneficial activities of transformed green ginseng berries has not reported elsewhere.
Methods: Ginsenosides of new green berry cultivar K-1 (GK-1) were identified by HPLC-QTOF/MS. Ginsenosides bioconversion in GK-1 by bgp1 enzyme was confirmed with HPLC and TLC. Then, mechanisms of GK-1 and β-glucosidase (bgp1) biotransformed GK-1 (BGK-1) were determined by Quantitative Reverse Transcription-Polymerase Chain Reaction and Western blot.
Results: GK-1 possesses highest ginsenosides especially ginsenoside-Re amongst seven ginseng cultivars including (Chunpoong, Huangsuk, Kumpoong, K-1, Honkaejong, Gopoong, and Yunpoong). Ginseng root's biomass is not affected with the harvest of GK-1 at 3 weeks after flowering period. Then, Re is bioconverted into a promising pharmaceutical effect of Rg2 *via* bgp1. According to the results of cell assays, BGK-1 shows decrease of tyrosinase and melanin content in α-melanocyte-stimulating hormone challenged-murine melanoma B16 cells. BGK-1 which is comparatively more effective than GK-1 extract shows significant suppression of the nuclear factor (NF)-κB activation and inflammatory target genes, in LPS-stimulated RAW 264.7 cells.
Conclusion: These results reported effective whitening and anti-inflammatory of BGK-1 as compared to GK-1.

1. Introduction

Ginseng (*Panax ginseng* Meyer, Araliaceae family) is a widely cultivated perennial plant in Korea and China for the frequent use of functional food and herbal medicine [1]. Ginseng berry (GB) is well known for its potential therapeutic effects mainly the biochemical and pharmacological properties including whitening [2], anticancer [1], anti-aging [3], and anti-diabetic [4]. The aforementioned effects are stimulated from the phytochemicals (ginsenosides, polysaccharides, amino acids, polyphenolics, fatty acids, and reducing sugars) that exist in GB [5–7]. In accordance with the beneficiary effect of various ginseng berry cultivars, the interest imposed in the field has drastically increased over the time.

GBs cultivars such as Chunpoong, Kumpoong, and Yunpoong were categorized according to variant physical representations (i.e., berry's color and stem) [8]. Yoon et al [9] reported that only the Kumpoong (yellow color berry) has the highest ginsenoside Rg1 as compared to other existing cultivars. A new cultivar, K-1 has been reported recently with its superior representation which has excellent root shape and strong disease resistance [10]. Apart from physical representation, chemical constituents (especially ginsenosides) existing in red ginseng berry (RGB) extract has been frequently studied [11,12]. However, the chemical components and biological activities of green (unripe) ginseng berry (GGB) extract

* Corresponding author. Graduate School of Biotechnology, and College of Life Science, Kyung Hee University, Yongin-si, Gyeonggi-do, Republic of Korea
E-mail address: yeonjukim@khu.ac.kr (Y.-J. Kim).

https://doi.org/10.1016/j.jgr.2021.02.007

Abbreviations

GK-1	Green berry cultivar K-1
bgp1	β-glucosidase
BGK-1	bgp1 biotransformed GK-1
RGB	Red ginseng berry
GGB	green ginseng berry
LPS	Lipopolysaccharide
NO	Nitric oxide
ROS	Reactive oxygen species
iNOS	Inducible nitric oxide synthase
TNF-α:	Tumor necrosis factor-α
IL-6	Interleukin 1 -6
IL-1β	Interleukin 1 beta
NF-κB	Nuclear factor kappa B
IκBα	Inhibitor kappa B-alpha
TLC	Thin-layer chromatography
HPLC	High-performance liquid chromatography
qRT-PCR	Quantitative Reverse transcription-polymerase chain reaction

are less reported as compared to RGB [13]. Whereby, Kim et al [14] reported that Re ginsenosides are abundantly found in both RGB and GGB.

Various methods for the Rg2 conversion from Re were proposed due to the promising enhancement of pharmaceutical effects such as heat processing [1], microwave and vinegar processing [14], and ultrasonication [15]. Apart from methods aforementioned, a novel approach of Rg2 conversion *via* biotransformation of Re was developed with recombinant β-glucosidase gene (bgp1) with promising productivity [16,17]. Whereby, bgp1 can be obtained from Microbacterium esteraromaticum which is commonly isolated from ginseng fields [18]. The bgp1 was generally cloned and represented in the form of *E.coli* BL21 (DE3) that comprises 2,496 base pairs bp (base pairs) and encoded with 831 amino acids. The minor ginsenoside conversion is done by the effective attachment on major ginsenosides after hydrolyzation of 1 glucose unit at C-20 position in ginsenoside aglycone by bgp1 enzyme.

The search for efficient and safe compounds from natural plants targeting skin treatment are frequently studied [19,20]. Generally, aging issues are the main target for skin treatment that leads to wrinkling, photo-aging, drying, roughness, lack of elasticity, and melanogenesis [21]. Specifically speaking, melanogenesis is an important skin protection factor that prevents harmful effects of solar radiation. However, abnormal accumulation of melanin would result in melasma and age spots [22]. Therefore, tyrosinase which controls the primary and rate-limiting processes of melanin production [23] shall be adopted to suppress melanogenesis that causes freckles and age spots.

Over-production of NO is important in inflammatory pathogenesis which would lead to cell damage by reacting with reactive oxygen species (ROS) [24,25]. Apart from that, nuclear factor kappa B (NF-κB) is a critical transcription cytokine that allows regulation of inflammatory factors [26]. In unstimulated cells, NF-κB is anchored in the cytoplasm as an inactive complex by inhibitor kappa B-alpha (IκBα) protein. However, RAW 264.7 cells stimulated by lipopolysaccharide (LPS), ubiquitination-mediated IκBα degradation results in NF-κB activation and nuclear translocation, which cause the transcription of inflammatory target genes such as TNF-α, IL-1β, and IL-6 [27].

In short, murine melanoma (B16) skin cells and LPS-stimulated RAW 264.7 cells in the presence of green new ginseng cultivar K-1 (GK-1) extract before and after bgp1-biotransformation were cultured. Then, cellular melanin content and tyrosinase action in the B16 cells was measured as well as the NO, ROS production, expression of NF-κB, IκBα proteins, TNF-α, IL-1β, inducible nitric oxide synthase (iNOS), and IL-6 genes level in the RAW 264.7 cells. To the extent of our knowledge, this is the first study considering biotransformation of GK-1 of saponins by bgp1, as well as the first report with the treatment on skin cells and RAW 264.7 with GK-1 and BGK-1 extract.

2. Materials and methods

2.1. Materials

The ginseng berries were provided by Gyeonggi Agricultural Research and Extension Services, South Korea. RAW 264.7 and B16 cell lines were provided by the Korean Cell Line Bank (Seoul, South Korea). Arbutin and L-3,4-dihydroxyphenylalanin (L-DOPA) were purchased from Abcam (Cambridge, UK), α-melanocyte-stimulating hormone (α-MSH), Lipopolysaccharide (LPS), and Griess were provided by Sigma (Sigma-Aldrich, St. Louis, MO, USA). Dulbecco Modified Eagle Medium (DMEM), fetal bovine serum (FBS), and antibiotics were supplied by GenDEPOT (Barker, TX, USA); 3-(4,5-dimethylthiazol-2yl)-2,5-diphenyltetrazolium bromide (MTT) was provided by Life Technologies (Eugene, OR). Antibodies of TNF-α, NF-κB, IκBα were provided by Cell Signal Technology (Danvers, MA, USA), genes primer sequence of TNF-α, IL-1β, IL-6 and iNOS designed by Macrogen (Seoul, South Korea). All other reagent-grade chemicals were purchased from commercial companies.

2.2. Preparation of bgp1 for GK-1 reaction

Recombinant enzymes were prepared according to a previously published method [18]. Briefly, bgp1 that was enriched in DE3 was transformed into recombinant bgp1. Then, bgp1 was cultured in the Luria-Bertani-ampicillin medium at 37 °C until it reached an optical density of 0.4 at 600 nm. 0.5 mM isopropyl-β-d-thiogalactopyranoside was added and incubated for an additional 9 h at 28 °C. The bacteria were collected by centrifugation process of 6,000 rpm for 15 min. The supernatant was harvested and stored at 4 °C until further experiments.

5 mL of bgp1 was reacted with an equal volume ratio of K-1 extract at 2.0 mg/mL in PBS and incubated under shaking (160 rpm) at 37 °C. An identical volume fraction of water-saturated n-butanol was added to each sample to inhibit the reaction. Herein, butanol was completely evaporated before ginsenosides analysis *via* TLC and HPLC.

2.3. Phytochemical analysis

Profiling of various ginsenosides in K-1 was carried out *via* flight-mass spectrometry (QTOF/MS) approach [28]. This analysis was executed in negative ion mode on Waters Xevo G2-S QTOF MS (Waters Corp., Milford, MA, USA). The MS detected the MSE acquisition mode data with alternative high- and low-collision energy scans using cone voltage and capillary settings of 40 V and 3.0 kV, respectively. The source temperature was 120 °C and desolvation temperature was 550 °C. The desolvation gas flow was 800 L/h, and cone gas flow was 30 L/h. Mass evaluations were performed by an automated calibration delivery system in the range between 100 m/z and 2,000 m/z.

The ginsenosides content was identified by HPLC (Agilent 1260, Palo Alto, CA, USA) [29]. In brief, seven cultivars powder were extracted with 70% ethanol then evaporated at 40 °C. The extracts were dissolved in 1 mL of methanol. The ginsenosides analysis was

established by HPLC in the C18 column at 203 nm with a 1.0 mL/min flow rate. Six individual ginsenosides were analyzed, and the ginsenoside-Rg1, -Re, -Rf, -Rg2, -Rb1, Rc, Rb2, F1, Rd as a reference. he period between 1st to 9th weeks of K-1 and BGK-1 were determined using HPLC. TLC evaluation was operated by silica gel 60 F254 plates from Merck KGaA (Darmstadt, Germany) in solvent mixture of chloroform-methanol-water with the volumetric ratio of 65:35:10 (v/v/v) as the developer. The spots on the TLC plates were stained by spraying them with sulfuric acid in ethanol (10:90, v/v), followed by reaction at 110 °C for 10 min.

Reducing sugar content in the K-1 extract was measured *via* the dinitrosalicylic acid (DNS) reagent approach [29]. K-1 extract and DNS reagent were mixed and boiled for 5 min, followed by a cool down process. The absorbance of the reaction mixture was measured at 550 nm by UV-reader (Bio-Tek, Winooski, VT) which glucose was used as reference. Total phenolic content in the K-1 extract was assessed by Folin-Ciocalteu approach [5]. K-1 extract dissolved in 1 mL methanol was mixed with 10% sodium carbonate for 3 min. Then, 1 mL of Folin-Ciocalteu reagent was incubated for 30 min. Total phenolic content of the GB samples was measured using UV-reader at 750 nm and determined based on calibration curves with gallic acid as reference. Acidic polysaccharides were analyzed with the extraction of 1 g K-1 in DW at 80 °C for 1 h. Then, ethanol was added and retained for reaction in 4 h periods to isolate polysaccharides from the mixture. Then, centrifugation, removal of supernatant, and evaporation at 40 °C. Acidic polysaccharides were measured by the m-hydroxydiphenyl method [30], which 0.2 mL of the sample was mixed with 1.2 mL of tetraborate-H2SO4 (12.5 mM) at 100 °C for 5 min. Finally, 20 μL of m-hydroxydiphenyl reagent was added and total polysaccharides were measured with UV-vis spectrophotometer at 550 nm.

2.4. Cell culture and viability assay

B16, and RAW 264.7 cells were incubated in DMEM supplemented with 10% FBS and 1% penicillin-streptomycin (100 ×) at 37 °C with a 95% humidified air and 5% CO_2 atmosphere [2]. Cell proliferation was executed *via* an MTT approach [31]. After cells were treated for 24 h, 100 μL of 0.5 mg/mL MTT reagent was added and cultured at 37 °C for additional 3 h. Next, 100 μL of DMSO was added and measurement of absorbance at 595 nm using SpectraMax ® ABS Plus microplate reader (Molecular Devices, San Jose, California, USA).

2.5. Cellular melanin content and tyrosinase activity assay

B16 cells were treated with α-MSH (100 nM), GK-1, BGK-1 (25 and 50 μg/mL) extracts for 72 h. The concentration of melanin in the B16 cells was assessed [32]. Cells were collected and the pellet was then solubilized in 500 μL of NaOH with 10% DMSO at 80 °C for 1 h. The absorbance was assessed at 475 nm using a microplate reader. The standard curve for synthetic melanin (0–500 μg/mL) was prepared in which the melanin production is presented as a percentage of the untreated control.

The activity of tyrosinase was measured using L-DOPA oxidative enzyme activity approach [32]. After B16 cells were treated, cells lysis with PBS containing 1% Triton X-100, and freeze-thawing at −80 °C for 15 min. After centrifugation at 12,000 rpm for 15 min, 10 μL of 15 mM L-DOPA was added to 90 μL of the lysate supernatant and incubated at 37 °C for 1 h. The tyrosinase activity was then evaluated absorbance at 475 nm by a microplate reader.

2.6. Measurement of NO and ROS production

The production of NO was determined by measuring nitrite levels with the Griess reagent [33]. RAW 264.7 cells were pretreated with different concentrations of GK-1, BGK-1 extract (25–100 μg/mL) or 1μM dexamethasone (DEX). After 1 h, cells were stimulated with 1 μg/mL of LPS. After 24 h incubation, the supernatant was mixed with the same volume of Griess reagent. NO levels were then determined using a microplate reader at 520 nm, and sodium nitrite concentrations were calculated by referencing a standard curve.

Intracellular accumulation of ROS was measured by executing cultivation in black 96-well plates. After RAW 264.7 cells were treated, 10 μM 5-chloromethyl-2,7-dichlorodihydrofluorescein diacetate were incubated for 30 min under the dark condition. Intracellular ROS generation was assessed and analyzed using a FLUO star OPTIMA fluorometer (BMG Labtech Inc.). The excitation and emission wavelengths were 485 nm and 535 nm, respectively. Cellular ROS Detection Analysis Kit was applied (Cambridge, MA, USA) were used to further confirm intracellular ROS generation. Raw 264.7 cells treated with GK-1 and BGK-1 for 24 h. 0.4 μL/mL of oxidative stress detection and superoxide detection reagents were added in cells. After 30 min stationed, fluorescence was measured by a laser scanning microscope (Leica, Wetzlar, Germany) and quantified using Image J software.

2.7. Immunofluorescence staining

The effect of GK-1 and BGK-1 on nuclear translocation of NF-kB p65 was assessed by immunofluorescence analysis. Raw 264.7 cells were fixed with 4% paraformaldehyde and permeabilization using 0.1% Triton X-100 for 20 min, then blocked with 2% BSA for 1 h. The antibodies of NF-κB p65 (1:500) were incubated for 3 h followed by 30 min incubation with fluorescein isothiocyanate (FITC)-conjugated secondary antibody. Nuclei were applied for Hoechst 33258 reagent, and fluorescence was snapped using a Leica fluorescence microscope and quantified using Image J software.

2.8. Quantitative reverse transcription-polymerase chain reaction (qRT-PCR)

Total RNA was obtained from RAW264.7 cells following a Trizol reagent kit instruction (Invitrogen, Carlsbad, CA, USA). First, 500 ng of total RNA was reverse transcribed with amfiRivert cDNA Synthesis Platinum Enzyme Mix (GenDEPOT, Katy, TX, USA). The reaction was performed at 60 °C for 1 min, 25 °C for 5 min, followed by 45 °C for 45 min, finally heating to 85 °C for 1 min using the CFX96TM Real Time RT-PCR System with SYBR PremixExTaqTM II (TaKaRa). qRT-PCR was performed using 50 ng cDNA in a 20 μL reaction volume using amfiSure qGreen Q-PCR Master Mix (GenDEOT, TX, USA). Gene-specific inflammatory-related primer sequences used for qRT-PCR are listed in Table S1. Glyceraldehyde-3-phosphate dehydrogenase (GAPDH) was used to normalize the expression level of inflammatory genes.

2.9. Western blot

GK-1 or BGK-1 extracts 50 and 100 μg/mL were incubated along with the LPS for 24 h. Cell pellets were harvested and lysed using a cell RIPA lysis buffer for 1 h, then centrifuged (12,000 rpm for 20 min). The protein concentration was quantified using the Bradford reagent (Sigma-Aldrich Co.). Hereby, an equal amount (50 μg) of total protein was loaded and resolved in 10% SDS-PAGE using an Invitrogen 2 mini electrophoresis tank system. Finally, it was transferred onto a PVDF membrane using iBlot™ 2 Gel Transfer

Device (Thermo Fisher Scientific, Massachusetts, USA). After 1 h of membrane blocking with 5% skim milk or BSA solution, the blots were incubated overnight with IκBα, p-IκBα, NF-κB p65, p-NF-κB p65 and β-actin at 4°C. The membranes were incubated with secondary antibodies for 1 h. Finally, signals were captured with West-Q pico Emitter Coupled Logic substrate (GenDEPOT, Texas, USA) and exposed to a Molecular Imager Gel DocTM XR + system (Bio-Rad Laboratories, Hercules, CA, USA). Protein band intensities were measured by Image J software.

2.10. Statistical analysis

All results were carried out in a triplicate manner and presented in the form of mean ± standard error of the mean (SEM). Statistical comparison between different treatments was assessed using the Student's t-test. $^{\#}P < 0.05$, $^{\#\#}P < 0.01$, and $^{\#\#\#}P < 0.001$ vs. control, and $P < 0.05$, $*P < 0.01$, and $**P < 0.001$ vs. α-MSH/LPS-stimulated control were indicated as statistically significant.

3. Results and discussion

3.1. Ginsenosides composition of different cultivars

Ginsenoside compositions in different ginseng berry cultivars were determined by HPLC analysis (Fig. 1A). As shown in Fig 1, K-1 has the highest total ginsenoside content (3.5 mg/g) among the available cultivars and Re was identified as the most abundant ginsenoside (Fig. 1B). Kumpoong (yellow berries) contained the highest Rg1 amongst other cultivars (Fig. 1B), but lowest Re among the others. Such finding has been supported by Yoon et al [9]. Anti-inflammatory activity of Kumpoong and K-1 were identified with the effect of LPS-induced NO production in RAW 264.7 cells. Negative cytotoxic effects were reported in the cell viability result (Fig. 1C) of Kumpoong and K-1 at the range below 100 μg/mL for both before and after biological transformation. Besides, bgp1-fermentation of Kumpoong and K-1 extract would efficiently enhance the suppression of LPS-stimulated NO production in every concentration (Fig. 1D). Notably, K-1 shows a better reduction effect of NO generation than that of Kumpoong. Therefore, K-1 cultivar was selected for further examination of its beneficiary properties.

3.2. Chemical composition comparison of K-1 for 4- and 5-years-old plant

K-1 berries that harvested between the 1st − 9th weeks after flowering and its granular form is shown in Fig. 2A. The weight of the harvested berries along the growth periods can be referred to Fig. 2B. Growth trend of ginseng roots during the harvest period is shown in Fig. 2C. Interestingly, the ratio of ginseng root weight started to increase at 3rd (+1.6%) and 4th (+1.0%) week after the decrement ratio (−1.4%) reported in 2nd week. Till then, the weight of the ginseng roots decreased from 5th week onwards and achieved the peak decrement (−8.3%) in 9th week. In short, appropriate harvest timeline for 4- and 5-years old green berries by considering high biological activity and least influence of ginseng roots' biomass are reported at 3rd and 2nd week, respectively. As per result of HPLC analysis (Fig. 2D), highest total ginsenosides content, especially Re (marked with yellow star) in both 4-and 5-years-old plants were reported at 3rd week and 2nd week, respectively. Nonetheless, in-house library of 63 ginsenosides for the K-1 ginsenosides profiling including name, exact mass, [M-H], [ESI-2], and [ESI-2] of each compound were developed with UNIFI software (version 1.7.1; Waters Corp., Milford, MA, USA). There are including 36 PPD types of ginsenosides, 25 PPT kinds of ginsenosides, and 2 Oleanolic (Table 1). The structures of all 63 types of ginsenoside based on the mass data were shown in Fig. S2. Surprisingly, the new cultivar of K-1 presented 38 more ginsenosides types than other cultivars (Chunpoong, Chungsun, Kumpoong, Yunpoong, Yunpoong, Gopoong, Sunwon, and Sunun) by QTOF/MS analysis [9].

Main bioactive constituents of K-1 which possess excellent pharmacological properties are reported with reducing sugars, flavonoids, phenolics, and acid polysaccharide [6,7,30]. Apart from that, organic acids, 5-C sugars and most of the ginsenosides were abundant during the pre-harvest (GGB) stages [34]. However, flavonoids and phenolic compounds would accumulate at higher levels in the later harvest/post-harvest stage. The concentration of reducing sugars were reported in the range of 15-20 mg/g (Fig. S1 A). Total flavonoid content (Fig. S1 B) in ripe berries (9th week) from 4-year-old plants was most abundant (160 mg/g). The amounts of total phenolics (Fig. S1 C) and acid polysaccharide (Fig. S1 D) were highest in the first 3 weeks of harvest period. Whereas, the highest total content of reducing sugars (Fig. S1 E) and acid polysaccharide (Fig. S1 H) for K-1 were reported at 2nd week for 5-year-old plants. The total flavonoids (Fig. S1F) and phenolic (Fig. S1G) were most abundant in the last 2 weeks of harvest period. In summary, K-1 from 5-year-old plants harvested during the 2nd week (unripe berries) contained the highest amount of total ginsenosides, reducing sugars, and acid polysaccharide. On the other hand, the total content of flavonoids and phenolic was highest in the last 2 weeks of harvesting period.

3.3. Ginsenoside alteration from Re to Rg2 in GK-1

As reported previously, Rg2 showed stronger neuro-protective [35] and obesity prevention [16] properties as compared to Re. Therefore, researchers were tempted to convert Re into the minor forms [1,36]. Several methods were proposed for Re deglycosylation into Rg2 including chemical [14], microbiological [37], physical [15], and heating [1]. However, most of the aforementioned methods have undesirable side effects. Herein, enzymatic conversion that discovered and proven previously are capable to address these side effects [18]. Therefore, bioconversion processes using the recombinant β-glucosidase (bgp1) were applied to convert Re into Rg2 through hydrolysis of glucose unit at C-20 position.

Ginsenoside bioconversion of Rg2 from Re *via* bgp1 fermentation (Fig. 2E and F) were executed from 2 different sample including 3rd and 2nd week of berries harvested from 4- and 5-years-old plants, respectively. Ginsenoside profiles were then analyzed with TLC and HPLC to validate the transformation after bgp1 bioconversion. In the TLC results (Fig. 2G), bands of Re on the plate decreased remarkably after biotransformation and the color band of the Rg2 is apparently deeper than that of the native ginsenoside Rg2. Whereas such result is validated by those reported in previous study by Huq et al [16]. In the HPLC results (Fig. 2H and I), the peak of Re almost disappeared after bgp1-fermentation and the Rg2 peak increased remarkably.

3.4. Whitening effect of GK-1 and BGK-1 in B16 cells

Melanin plays an essential role in protecting skin against the harmful effects of solar radiation, but it's abnormal accumulation would lead to melasma and age spots [38]. Generally, melanogenesis is initiated by tyrosinase-catalyzed oxidation process [39]. Herein, cytotoxicity of GK-1 and BGK-1 extracts in B16 cells after 24 h exposure were evaluated with MTT. In results, there were no significant cytotoxic effect reported at any treatment concentration in B16 cells (Fig. 3A). Hereby, whitening effects were examined with the melanin and tyrosinase after GK-1 and BGK-1 treatment in α-MSH-challenged cells. As for melanin production, dosage

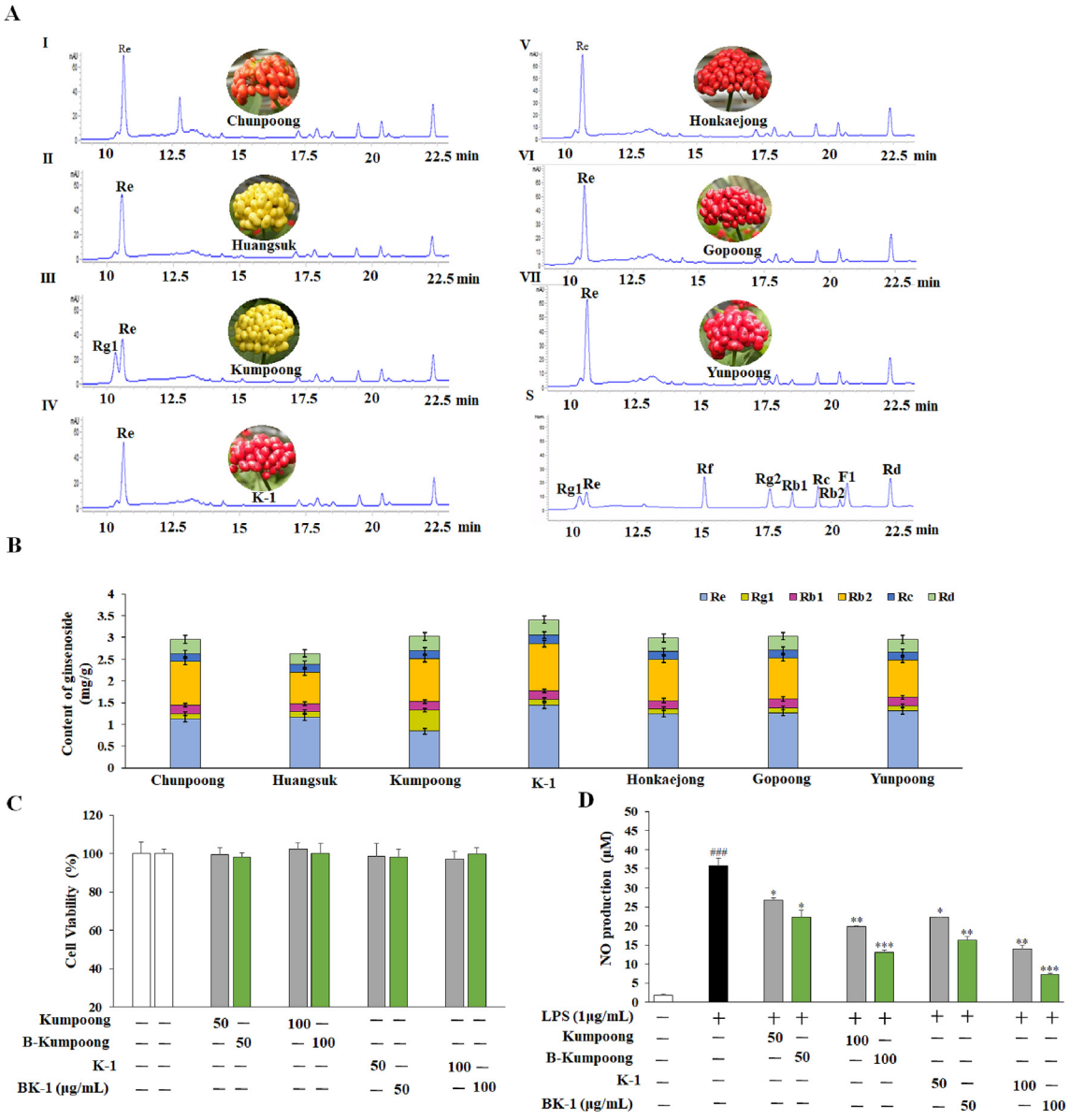

Fig. 1. Physicochemical properties and anti-inflammatory effect of biotransformed ginseng berries. 7 types of ginseng cultivar's ginsenosides contents were determined *via* HPLC along with Morphological characteristics (A); Total available ginsenoside concentrations in ginseng berries (B). RAW 264.7 cells incubation with various concentrations of Kumpoong and K-1 extracts before exposure to 1μg/mL of LPS for 24 h (C); NO production (D). Data are expressed as the mean ± SEM. $^{\#}P < 0.05$, $^{\#\#}P < 0.01$, and $^{\#\#\#}P < 0.001$ vs. control. $P < 0.05$,*$P < 0.01$, and**$P < 0.001$ vs. LPS-treated control.

dependencies were reported with significant reduction (Fig. 3B). Suppression effect of the treatment with 25 and 50 μg/mL of GK-1 and BGK-1 extracts shows higher suppression effect as compared to arbutin treatment at 50 μg/mL. Whereby, BGK-1 extract was reported with higher effectiveness in reducing cellular melanin content than that of GK-1 extract at both concentrations. On the other hand, cellular tyrosinase activity increased significantly solely with α-MSH while comparing with other untreated cells. However, GK-1 and BGK-1 extracts treatment would significantly suppress the increase of α-MSH-caused tyrosinase activity. BGK-1 extracts were reported with effective suppression of intracellular tyrosinase activity while compared to GK-1 extract at 25 and 50 μg/mL (Fig. 3C). Therefore, GK-1 was suggested as potential therapeutic option to suppress α-MSH-stimulated melanin production.

3.5. NO production and iNOS gene expression

Cytotoxicity of RAW 264.7 cells after treatment were tested with indicated concentrations of GK-1 and BGK-1 extract (25–100 μg/mL) *via* MTT. In return, GGB extract did not exhibit any significant cytotoxic effect on RAW 264.7 cells in the maximum range of 100 μg/mL (Fig. 4A). Then, effect of GK-1 and BGK-1 that stimulated by LPS on NO production and iNOS gene expression were examined. Whereby, NO is commonly identified as activator that synthesized by nitric oxide synthases. As shown in Fig. 4B, LPS would significantly increase the NO production in RAW 264.7 cells. Both GK-1 and BGK-1 extracts show only slight inhibition on the LPS-induced NO production at 25 μg/mL. However, it then shows remarkable suppression from 50 μg/mL to 100 μg/mL ($P < 0.01$) in dosage-dependent manner. Notably, BGK-1 extract shows better

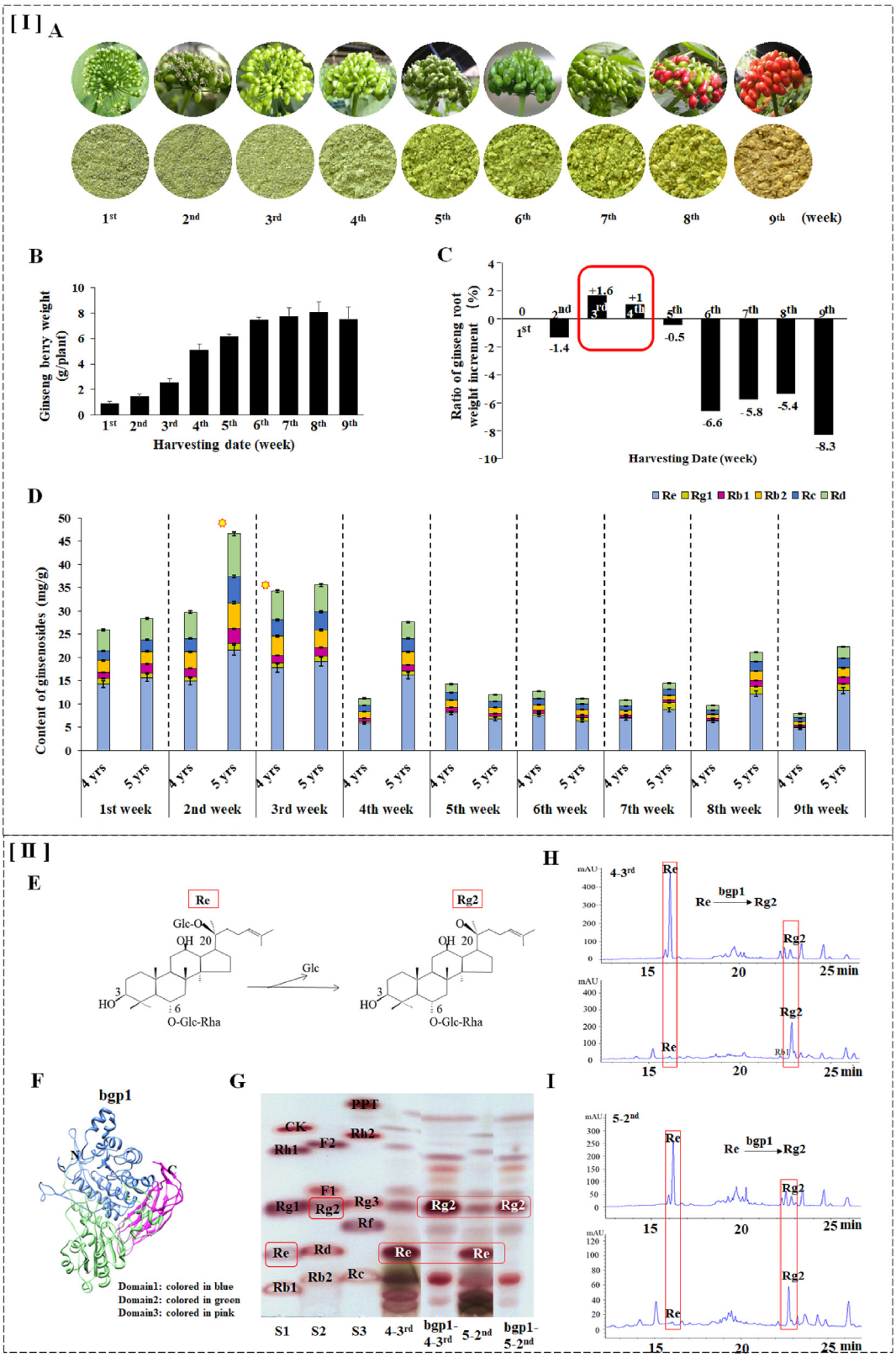

Fig. 2. [I] Physical properties of K-1 berries in different growth periods along with K-1's available ginsenoside contents comparison between 4- and 5-year-old plants. [II] Ginsenosides bioconversion in GK-1 and transformation scheme of Re by bgp1-treatment. granular form of K-1 from 1st – 9th week (A); Weight of ginseng berries (B); Ginseng root biomass profile (C); Ginsenoside profiles and content in K-1 from 4-years and 5-years old plants (D). -Glc: D-glucopyranosyl, -Rha: L-rhamnopyranosyl (E); Three dimensional structure of bgp1 (F); TLC profiles of Re and Rg2 in GK1 and BGK-1 (G); HPLC profiles of Re and Rg2 in GK1 and BGK-1 from 4-year-old plants (H); HPLC profiles of Re and Rg2 in GK1 and BGK-1 from 5-year-old plants (I).

Table1
In-house Library of 63 ginsenosides Created Using QTOF/MS data

Type	Name	Exact mass	[M-H]	[ESI-2]	[ESI+44]	Type	Name	Exact mass	[M-H]	[ESI-2]	[ESI+44]
PPD	Compound K	622.44447	621.43664	620.64	666.44	PPT	ginsenoside A1	800.49221	799.48438	798.69	844.49
PPD	ginsenoside F2	784.49729	783.48946	782.70	828.50	PPT	ginsenoside F1	638.43938	637.43155	636.64	682.44
PPD	ginsenoside I	978.53995	977.53212	976.74	1022.54	PPT	ginsenoside F3	800.49221	799.48438	798.69	844.49
PPD	ginsenoside La	782.48164	781.47381	780.68	826.48	PPT	ginsenoside F4	766.48673	765.47890	764.69	810.49
PPD	ginsenoside Mc	786.45880	785.45097	784.66	830.46	PPT	ginsenoside Ia	800.49221	799.48438	798.69	844.49
PPD	ginsenoside Ra1	1126.62955	1125.62172	1124.83	1170.63	PPT	ginsenoside Re	946.55012	945.54229	944.75	990.55
PPD	ginsenoside Ra2	1210.63463	1209.62680	1208.83	1254.63	PPT	ginsenoside Rf	800.49221	799.48438	798.69	844.49
PPD	ginsenoside Ra3	1256.64011	1255.63228	1254.84	1300.64	PPT	ginsenoside Rg1	800.49221	799.48438	798.69	844.49
PPD	ginsenoside Rb1	1108.60294	1107.59511	1106.80	1152.60	PPT	ginsenoside Rg2	784.49729	783.48946	782.70	828.50
PPD	ginsenoside Rb2 α-L-arabinose	1078.59237	1077.58454	1076.79	1122.59	PPT	ginsenoside Rg8	798.47656	797.46873	796.68	842.48
PPD	ginsenoside Rb3	1064.57672	1063.56889	1062.78	1108.58	PPT	ginsenoside Rh1	638.43938	637.43155	636.64	682.44
PPD	ginsenoside Rc	1078.59237	1077.58454	1076.79	1122.59	PPT	ginsenoside Rh4	620.42882	619.42099	618.63	664.43
PPD	ginsenoside Rd2	916.53955	915.53172	914.74	960.54	PPT	ginsenoside Rk3	620.42882	619.42099	618.63	664.43
PPD	ginsenoside Rg3	784.49729	783.48946	782.70	828.50	PPT	gynosaponin TN-1	654.43430	653.42647	652.63	698.43
PPD	ginsenoside Rg5	766.48673	765.47890	764.69	810.49	PPT	gypenoside I-EH	1108.60294	1107.59511	1106.80	1152.60
PPD	ginsenoside Rh2	622.44447	621.43664	620.64	666.44	PPT	kroyoginsenoside R1	868.51842	867.51059	866.72	912.52
PPD	ginsenoside Rk1	766.48673	765.47890	764.69	810.49	PPT	notoginsenoside H	948.52938	947.52155	946.73	992.53
PPD	ginsenoside Rs1	1136.59785	1135.59002	1134.80	1180.60	PPT	notoginsenoside J	818.50277	817.49494	816.70	862.50
PPD	ginsenoside S	946.55012	945.54229	944.75	990.55	PPT	notoginsenoside R1	932.53447	931.52664	930.73	976.53
PPD	gynosaponin I	946.55012	945.54229	944.75	990.55	PPT	notoginsenoside R2	770.48164	769.47381	768.68	814.48
PPD	gynosaponin M	784.49729	783.48946	782.70	828.50	PPT	notoginsenoside R3	946.55012	945.54229	944.75	990.55
PPD	kroyoginsenoside R2	1124.59785	1123.59002	1122.80	1168.60	PPT	notoginsenoside R8	654.43430	653.42647	652.63	698.43
PPD	malonyl ginsenoside Rb2	1194.60333	1193.59550	1192.80	1238.60	PPT	notoginsenoside R9	654.43430	653.42647	652.63	698.43
PPD	malonyl ginsenoside Rc	1164.59277	1163.58494	1162.79	1208.59	PPT	notoginsenoside ST-1	654.43430	653.42647	652.63	698.43
PPD	malonyl ginsenoside Rd	1048.54542	1047.53759	1046.75	1092.55	PPT	pseudoginsenoside F8	1136.59785	1135.59002	1134.80	1180.60
PPD	malonyl ginsenoside Rd1	1194.60333	1193.59550	1192.80	1238.60	Oleanolic	ginsenoside RO	956.49808	955.49025	954.70	1000.50
PPD	notoginsenoside A	1124.59785	1123.59002	1122.80	1168.60	Oleanolic	ginsenoside ROA	1118.55090	1117.54307	1116.75	1162.55
PPD	notoginsenoside B	1094.55090	1093.54307	1092.75	1138.55						
PPD	notoginsenoside C	1140.59277	1139.58494	1138.79	1184.59						
PPD	notoginsenoside E	978.53995	977.53212	976.74	1022.54						
PPD	notoginsenoside Fe	900.54464	899.53681	898.74	944.54						
PPD	notoginsenoside G	960.52938	959.52155	958.73	1004.53						
PPD	notoginsenoside I	1092.60802	1091.60019	1090.81	1136.61						
PPD	notoginsenoside ST-2	830.50277	829.49494	828.70	874.50						
PPD	notoginsenoside ST-3	830.50277	829.49494	828.70	874.50						
PPD	notoginsenoside ST-5	916.53955	915.53172	914.74	960.54						

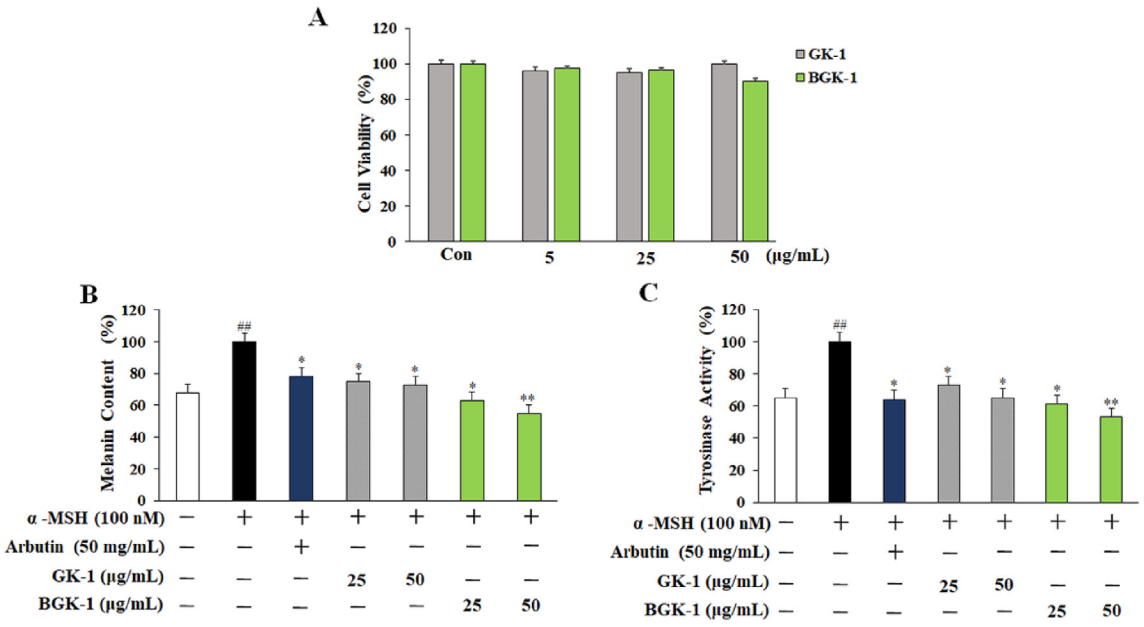

Fig. 3. Whitening effect of GK-1 and BGK-1 in B16 cells which incubated in different concentrations (5 to 50 μg/mL) with 100 nM α-MSH for 72 h. Cell viability was determined by MTT assay. Cytotoxicity in B16 melanoma cells (A); Melanin content (B); Tyrosinase activity assay (C). Data are presented as the mean ± SEM. $^{\#}P < 0.05$, $^{\#\#}P < 0.01$, and $^{\#\#\#}P < 0.001$ vs. control. $P < 0.05$, $^{*}P < 0.01$, and $^{**}P < 0.001$ vs. α-MSH -stimulated control.

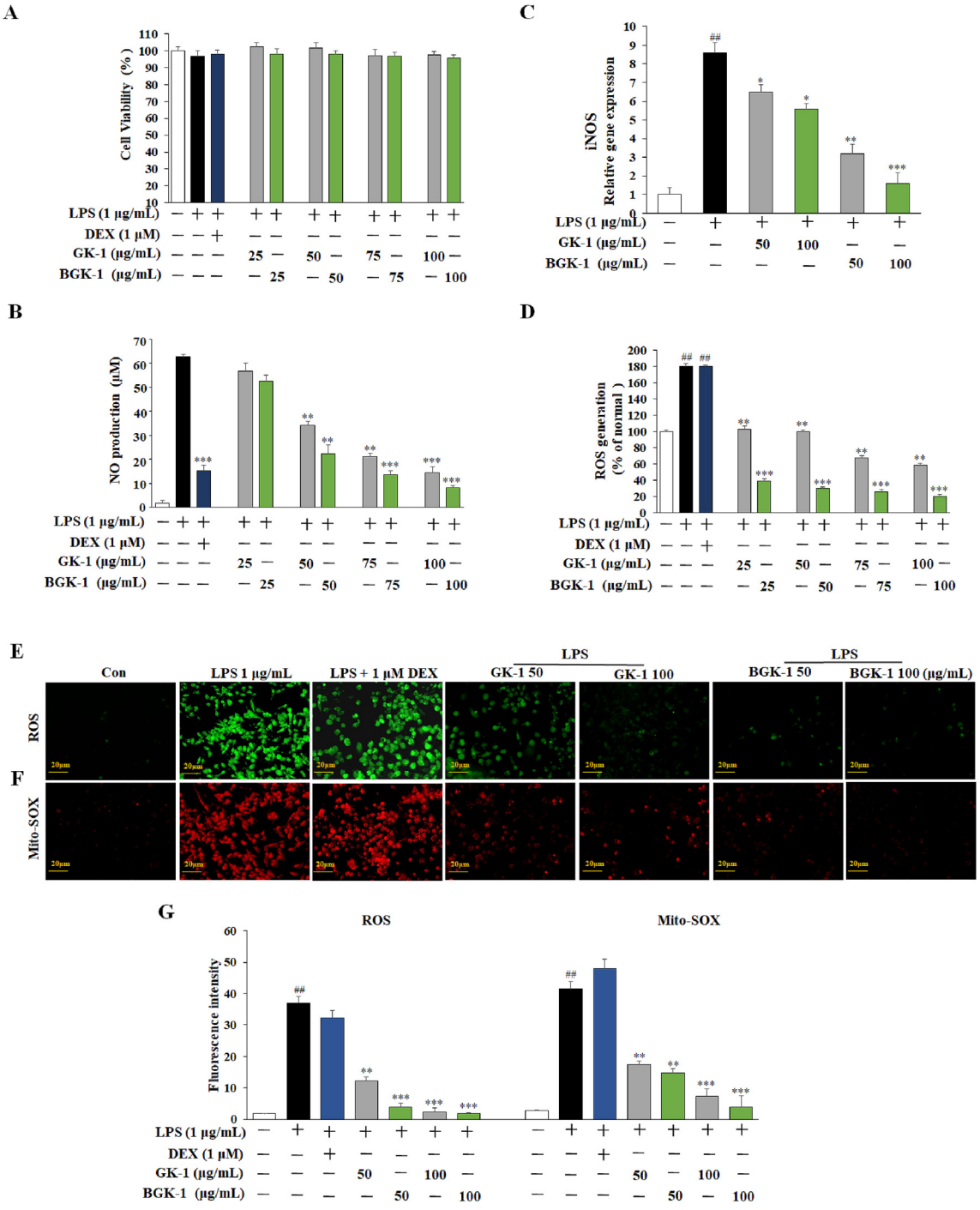

Fig. 4. Inflammation suppression of GK-1 and BGK-1 in distinct treatment concentration on RAW 264.7 cells with different LPS mode (1 μg/mL) for 24 h. Cytotoxicity in RAW 264.7 cells (A); Production of NO (B); iNOS gene expression *via* qRT-PCR (C); ROS generation assay (D); Oxidative stress detection (E) and superoxide detection (F) *via* immunofluorescence staining; ROS and Mito-SOX fluorescence intensity (G). Data are expressed as the mean ± SEM. $^{\#}P < 0.05$, $^{\#\#}P < 0.01$, and $^{\#\#\#}P < 0.001$ vs. control. P < 0.05,*P < 0.01, and**P < 0.001 vs. LPS-treated control.

reduction of NO production than GK-1 extract at both 50 μg/mL and 100 μg/mL.

iNOS which regulated by stimulated cytokines were reported with active involvement in immune response that would catalyze NO production [40]. As reported previously, iNOS expression increment would induce transcriptional activation in RAW 264.7 cells [41]. Therefore, management of NO and iNOS levels is essential for anti-inflammation. In our study, production of iNOS accumulation by LPS in RAW 264.7 cells were assessed by qRT-PCR analysis. LPS shows remarkable increase of iNOS gene expression in RAW 264.7 cells (Fig. 4C). Whilst, iNOS production was inhibited when RAW 264.7 cells were treated with GK-1 and BGK-1 (50 and 100 μg/mL). Overall, BGK-1 extract was more effective in reducing iNOS gene expression than that of GK-1 extract at both concentrations aforementioned.

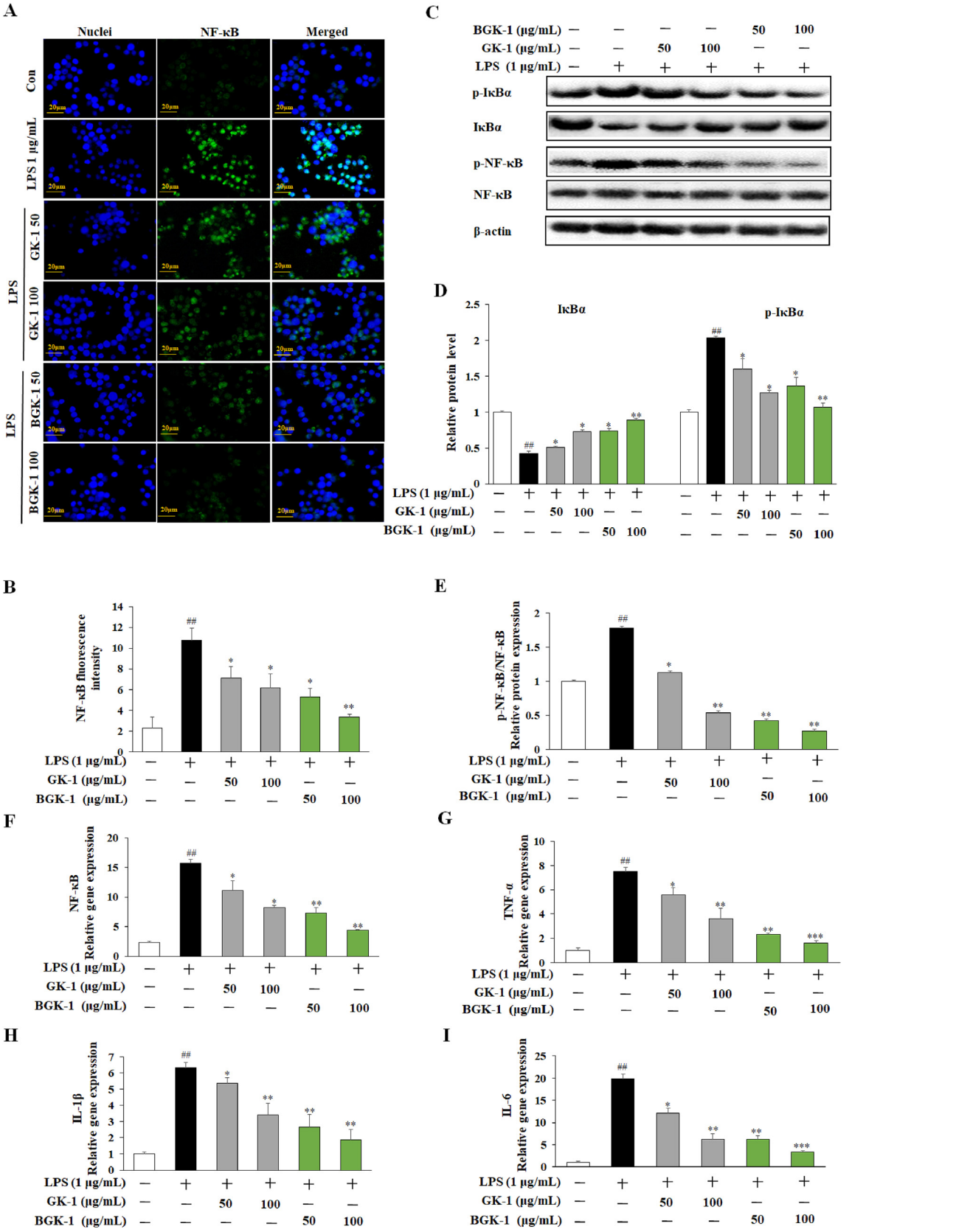

Fig. 5. Inflammation suppression of GK-1 and BGK-1 in distinct treatment concentration on RAW 264.7 cells with different LPS mode (1 μg/mL) for 24 h. Immunofluorescence analysis of NF-kB p65 nuclear translocation (A): RAW 264.7 cells were stained with anti-p65-NF-kB (green), nucleus was stained with Hoechst 33258 (blue), and merge image represented p65 nuclear transfer; NF-kB fluorescence intensity (B); Western blot analysis on the expressions of IκBα, p-IκBα, NF-κB and p-NF-κB (C); Bands intensity value were quantified and normalized to the corresponding β-actin: p-IκBα and IκBα (D); p-NF-κB/NF-κB (E). Genes expression evaluation in LPS-challenged RAW 267.4 cells *via* qRT-PCR: NF-κB gene expression (F); TNF-α gene expression (G); IL-1β gene expression (H); IL-6 gene expression (I). Data are expressed as the mean ± SEM. $^{\#}P < 0.05$, $^{\#\#}P < 0.01$, and $^{\#\#\#}P < 0.001$ vs. control. $P < 0.05$,*$P < 0.01$, and**$P < 0.001$ vs. LPS-treated control.

3.6. ROS production

ROS is an important regulator of intracellular signaling and homeostasis with chemically reactive molecules with oxygen. Generally, ROS would accumulate during the exposure of LPS which leads to critical cell damage [42]. Therefore, examinations were carried out on both LPS-induced GK-1 and BGK-1 extracts on ROS production inhibition. In result, LPS shows remarkable increment of ROS production compared with untreated control, and over-production was significantly suppressed by treatment with the GK-1 and BGK-1 extracts in concentration dependent manner ($p < 0.05$ or $p < 0.01$). Generally, BGK-1 extract shows superior reduction effect of ROS generation at any concentration as compared to GK-1 extract (Fig. 4D). Yet, the DEX (1 μM) group increased the ROS and superoxide generation as compared to the control group. The finding was further supported by previous studies [43,44]. Notably, NO generation was reported with slight reduction with the increase of intracellular ROS levels after Dex (1 uM) group, which the result was aliased with previous studies [45,46]. Conclusively, GK-1 and BGK-1 could inhibit LPS-challenged ROS accumulation in macrophages. The staining of ROS (Fig. 4E) and superoxide generation (Fig. 4F) along with the fluorescence intensity (Fig. 4G) are presented.

3.7. Activation inhibition of NF-κB signaling pathway

NF-κB dimer is bound within its inhibitory protein IκBα in the cytoplasm which the phosphorylated IκBα is ubiquitinated and degraded once stimulated by LPS, followed by nuclear translocation of NF-κB occurs, which leads to the transcription of inflammation genes such as TNF-α, IL-1β, and IL-6 [40]. According to the molecular mechanism from previous studies, phosphorylated and degraded IκBα would lead to the rise towards the activation of NF-κB in LPS-induced RAW 264.7 cells [26,27]. The immunofluorescence staining of NF-κB (Fig. 5A) and its respected intensity (Fig. 5B) are shown. Hereby, LPS stimulated cells showed remarkable induced of phosphorylated IκB-α which indicates degradation of IκB-α and NF-κB complex and inflammatory target genes. However, treatment with GK-1 and BGK-1 extracts decreased with degradation of IκB-α and NF-κB complex by inhibiting the phosphorylation of these 2 genes (Fig. 5C–E) and inflammatory target genes such as TNF-α, IL-1β, and IL-6 (Fig. 5F–H). In addition, BGK-1 extract was found to be more effective to suppress inflammatory than GK-1 extract at both 50 μg/mL and 100 μg/mL. Therefore, the GK-1 and BGK-1 extracts are concluded with the anti-inflammation properties.

4. Conclusion

Feasible harvesting time for ginseng berries without negatively affecting the root biomass is suggested as according to: 3rd week for 4 year and 2nd week for 5 year old ginseng. The ginsenoside Re extracted from new cultivar K-1 green berries can be transformed into more pharmacologically active Rg2 using recombinant β-glucosidase (bgp1). Our results have clearly indicated that bgp1-biotransformed green K-1 berries (BGK-1) can suppress tyrosinase and melanin content in α-MSH-stimulated B16 cells and are comparatively more effective than that of the original GK-1. We also validated that the anti-inflammatory effect of GK-1 and BGK-1 extracts was thought to work by inhibiting NO, ROS production, and NF-κB activation, followed by inflammatory genes such as TNF-α, IL-1β, and IL-6 in LPS-challenged RAW 264.7 cells. In summary, bgp1-biotransformed green ginseng berries of new cultivar K1 have increased the whitening effect on skin cells and enhanced the anti-inflammatory activity dramatically by reducing NF-κB-mediated inflammation.

Declaration of competing interest

The authors declare that they have no conflict of interest regarding this publication.

Acknowledgments

This work was supported by the Rural Development Administration grant “Cooperative Research Program for Agriculture Science and Technology Development (Project No. PJ013173))”, and grant from Basic Science Research Program through National Research Foundation of Korea by Ministry of Education (2019R1A2C1010428), Republic of Korea.

Appendix A. Supplementary data

Supplementary data to this article can be found online at https://doi.org/10.1016/j.jgr.2021.02.007.

References

[1] Jang HJ, Han IH, Kim YJ, Yamabe N, Lee D, Hwang GS, et al. Anticarcinogenic effects of products of heat-processed ginsenoside Re, a major constituent of ginseng berry, on human gastric cancer cells. J Agric Food Chem 2014;62:2830–6. https://doi.org/10.1021/jf5000776.
[2] Jiménez Z, Kim Y-J, Mathiyalagan R, Seo K-H, Mohanan P, Ahn J-C, et al. Assessment of radical scavenging, whitening and moisture retention activities of Panax ginseng berry mediated gold nanoparticles as safe and efficient novel cosmetic material. Artif Cells, Nanomedicine, Biotechnol 2018;46:333–40. https://doi.org/10.1080/21691401.2017.1307216.
[3] Kim J, Cho SY, Kim SH, Cho D, Kim S, Park CW, et al. Effects of Korean ginseng berry on skin antipigmentation and antiaging via FoxO3a activation. J Ginseng Res 2017;41:277–83. https://doi.org/10.1016/j.jgr.2016.05.005.
[4] Li Z, Kim HJ, Park MS, Ji GE. Effects of fermented ginseng root and ginseng berry on obesity and lipid metabolism in mice fed a high-fat diet. J Ginseng Res 2018;42:312–9. https://doi.org/10.1016/j.jgr.2017.04.001.
[5] Chung IM, Lim JJ, Ahn MS, Jeong HN, An TJ, Kim SH. Comparative phenolic compound profiles and antioxidative activity of the fruit, leaves, and roots of Korean ginseng (Panax ginseng Meyer) according to cultivation years. J Ginseng Res 2016;40:68–75. https://doi.org/10.1016/j.jgr.2015.05.006.
[6] Wang CZ, Hou L, Wan JY, Yao H, Yuan J, Zeng J, et al. Ginseng berry polysaccharides on inflammation-associated colon cancer: inhibiting T-cell differentiation, promoting apoptosis, and enhancing the effects of 5-fluorouracil. J Ginseng Res 2020;44:282–90. https://doi.org/10.1016/j.jgr.2018.12.010.
[7] Parikh M, Raj P, Yu L, Stebbing JA, Prashar S, Petkau JC, et al. Ginseng berry extract rich in phenolic compounds attenuates oxidative stress but not cardiac remodeling post myocardial infarction. Int J Mol Sci 2019;20. https://doi.org/10.3390/ijms20040983.
[8] Kim SW, Gupta R, Lee SH, Min CW, Agrawal GK, Rakwal R, et al. An integrated biochemical, proteomics, and metabolomics approach for supporting medicinal value of panax ginseng fruits. Front Plant Sci 2016;7:994. https://doi.org/10.3389/fpls.2016.00994.
[9] Yoon D, Choi B-R, Kim Y-C, Oh SM, Kim H-G, Kim J-U, et al. Comparative analysis of panax ginseng berries from seven cultivars using UPLC-QTOF/MS and NMR-based metabolic profiling. Biomolecules 2019;9. https://doi.org/10.3390/biom9090424.
[10] Wang H, Xu F, Wang X, Kwon WS, Yang DC. Molecular discrimination of Panax ginseng cultivar K-1 using pathogenesis-related protein 5 gene. J Ginseng Res 2019;43:482–7. https://doi.org/10.1016/j.jgr.2018.07.001.
[11] Bae HM, Cho OS, Kim SJ, Im BO, Cho SH, Lee S, et al. Inhibitory effects of ginsenoside re isolated from ginseng berry on histamine and cytokine release in human mast cells and human alveolar epithelial cells. J Ginseng Res 2012;36:369–74. https://doi.org/10.5142/jgr.2012.36.4.369.
[12] Nam Y, Bae J, Jeong JH, Ko SK, Sohn UD. Protective effect of ultrasonication-processed ginseng berry extract on the D-galactosamine/lipopolysaccharide-

induced liver injury model in rats. J Ginseng Res 2018;42:540–8. https://doi.org/10.1016/j.jgr.2017.07.007.
[13] Park EY, Kim HJ, Kim YK, Park SU, Choi JE, Cha JY, et al. Increase in insulin secretion induced by panax ginseng berry extracts contributes to the amelioration of hyperglycemia in streptozotocininduced diabetic mice. J Ginseng Res 2012;36:153–60. https://doi.org/10.5142/jgr.2012.36.2.153.
[14] Kim SJ, Kim JD, Ko SK. Changes in ginsenoside composition of ginseng berry extracts after a microwave and vinegar process. J Ginseng Res 2013;37:269–72. https://doi.org/10.5142/jgr.2013.37.269.
[15] Jung H, Bae J, Ko SK, Sohn UD. Ultrasonication processed Panax ginseng berry extract induces apoptosis through an intrinsic apoptosis pathway in HepG2 cells. Arch Pharm Res 2016;39:855–62. https://doi.org/10.1007/s12272-016-0760-6.
[16] Huq MA, Siraj FM, Kim YJ, Yang DC. Enzymatic transformation of ginseng leaf saponin by recombinant beta-glucosidase (bgp1) and its efficacy in an adipocyte cell line. Biotechnol Appl Biochem 2016;63:532–8. https://doi.org/10.1002/bab.1400.
[17] Quan L-H, Min J-W, Yang D-U, Kim Y-J, Yang D-C. Enzymatic biotransformation of ginsenoside Rb1 to 20(S)-Rg3 by recombinant β-glucosidase from Microbacterium esteraromaticum. Appl Microbiol Biotechnol 2012;94:377–84. https://doi.org/10.1007/s00253-011-3861-7.
[18] Quan LH, Min JW, Sathiyamoorthy S, Yang DU, Kim YJ, Yang DC. Biotransformation of ginsenosides Re and Rg1 into ginsenosides Rg2 and Rh1 by recombinant beta-glucosidase. Biotechnol Lett 2012;34:913–7. https://doi.org/10.1007/s10529-012-0849-z.
[19] Mack Correa MC, Mao G, Saad P, Flach CR, Mendelsohn R, Walters RM. Molecular interactions of plant oil components with stratum corneum lipids correlate with clinical measures of skin barrier function. Exp Dermatol 2014;23:39–44. https://doi.org/10.1111/exd.12296.
[20] van Smeden J, Bouwstra JA. Stratum corneum lipids: their role for the skin barrier function in healthy subjects and atopic dermatitis patients. Curr Probl Dermatol 2016;49:8–26. https://doi.org/10.1159/000441540.
[21] Ando H, Niki Y, Ito M, Akiyama K, Matsui MS, Yarosh DB, et al. Melanosomes are transferred from melanocytes to keratinocytes through the processes of packaging, release, uptake, and dispersion. J Invest Dermatol 2012;132:1222–9. https://doi.org/10.1038/jid.2011.413.
[22] Pereira AFC, Igarashi MH, Mercuri M, Pereira AF, Pinheiro A, da Silva MS, et al. Whitening effects of cosmetic formulation in the vascular component of skin pigmentation. J Cosmet Dermatol 2019. https://doi.org/10.1111/jocd.12979.
[23] Thong HY, Jee SH, Sun CC, Boissy RE. The patterns of melanosome distribution in keratinocytes of human skin as one determining factor of skin colour. Br J Dermatol 2003;149:498–505.
[24] Nomura J, Busso N, Ives A, Tsujimoto S, Tamura M, So A, et al. Febuxostat, an inhibitor of xanthine oxidase, suppresses lipopolysaccharide-induced MCP-1 production via MAPK phosphatase-1-mediated inactivation of JNK. PLoS One 2013;8:e75527. https://doi.org/10.1371/journal.pone.0075527.
[25] Quinonez-Flores CM, Gonzalez-Chavez SA, Del Rio Najera D, Pacheco-Tena C. Oxidative stress relevance in the pathogenesis of the rheumatoid arthritis: a systematic review. Biomed Res Int 2016;2016:6097417. https://doi.org/10.1155/2016/6097417.
[26] Yu HS, Lee NK, Choi AJ, Choe JS, Bae CH, Paik HD. Anti-inflammatory potential of probiotic strain weissella cibaria JW15 isolated from kimchi through regulation of NF-kappaB and MAPKs pathways in LPS-induced RAW 264.7 cells. J Microbiol Biotechnol 2019;29:1022–32. https://doi.org/10.4014/jmb.1903.03014.
[27] Zhao Z, Dai XS, Wang ZY, Bao ZQ, Guan JZ. MicroRNA-26a reduces synovial inflammation and cartilage injury in osteoarthritis of knee joints through impairing the NF-kappaB signaling pathway. Biosci Rep 2019;39. https://doi.org/10.1042/BSR20182025.
[28] Lee JW, Ji SH, Lee YS, Choi DJ, Choi BR, Kim GS, et al. Mass spectrometry based profiling and imaging of various ginsenosides from panax ginseng roots at different ages. Int J Mol Sci 2017;18. https://doi.org/10.3390/ijms18061114.
[29] Jin Y, Kim YJ, Jeon JN, Wang C, Min JW, Noh HY, et al. Effect of white, red and black ginseng on physicochemical properties and ginsenosides. Plant Foods Hum Nutr 2015;70:141–5. https://doi.org/10.1007/s11130-015-0470-0.
[30] Kim M, Yi Y-S, Kim J, Han SY, Kim SH, Seo DB, et al. Effect of polysaccharides from a Korean ginseng berry on the immunosenescence of aged mice. J Ginseng Res 2018;42:447–54. https://doi.org/10.1016/j.jgr.2017.04.014.
[31] Park JS, Park EM, Kim DH, Jung K, Jung JS, Lee EJ, et al. Anti-inflammatory mechanism of ginseng saponins in activated microglia. J Neuroimmunol 2009;209:40–9. https://doi.org/10.1016/j.jneuroim.2009.01.020.
[32] Wang DD, Jin Y, Wang C, Kim YJ, Perez ZEJ, Baek NI, et al. Rare ginsenoside Ia synthesized from F1 by cloning and overexpression of the UDP-glycosyltransferase gene from Bacillus subtilis: synthesis, characterization, and in vitro melanogenesis inhibition activity in BL6B16 cells. J Ginseng Res 2018;42:42–9. https://doi.org/10.1016/j.jgr.2016.12.009.
[33] Wang PF, Li YP, Ding LQ, Cao SJ, Wang LN, Qiu F. Six new methyl apiofuranosides from the bark of phellodendron chinense schneid and their inhibitory effects on nitric oxide production. Molecules 2019;24. https://doi.org/10.3390/molecules24101851.
[34] Sreekanth TVM, Nagajyothi PC, Muthuraman P, Enkhtaivan G, Vattikuti SVP, Tettey CO, et al. Ultra-sonication-assisted silver nanoparticles using Panax ginseng root extract and their anti-cancer and antiviral activities. J Photochem Photobiol B 2018;188:6–11. https://doi.org/10.1016/j.jphotobiol.2018.08.013.
[35] Chen J, Li M, Qu D, Sun Y. Neuroprotective effects of red ginseng saponins in scopolamine-treated rats and activity screening based on pharmacokinetics. Molecules 2019;24. https://doi.org/10.3390/molecules24112136.
[36] Kim ST, Kim HB, Lee KH, Choi YR, Kim HJ, Shin IS, et al. Steam-dried ginseng berry fermented with Lactobacillus plantarum controls the increase of blood glucose and body weight in type 2 obese diabetic db/db mice. J Agric Food Chem 2012;60:5438–45. https://doi.org/10.1021/jf300460g.
[37] Li Z, Ahn HJ, Kim NY, Lee YN, Ji GE. Korean ginseng berry fermented by mycotoxin non-producing Aspergillus Niger and Aspergillus oryzae: ginsenoside analyses and anti-proliferative activities. Biol Pharm Bull 2016;39:1461–7. https://doi.org/10.1248/bpb.b16-00239.
[38] Solano F, Briganti S, Picardo M, Ghanem G. Hypopigmenting agents: an updated review on biological, chemical and clinical aspects. Pigment Cell Res 2006;19:550–71. https://doi.org/10.1111/j.1600-0749.2006.00334.x.
[39] Hearing VJ. Determination of melanin synthetic pathways. J Invest Dermatol 2011;131:E8–11. https://doi.org/10.1038/skinbio.2011.4.
[40] Zhai XT, Zhang ZY, Jiang CH, Chen JQ, Ye JQ, Jia XB, et al. Nauclea officinalis inhibits inflammation in LPS-mediated RAW 264.7 macrophages by suppressing the NF-kappaB signaling pathway. J Ethnopharmacol 2016;183:159–65. https://doi.org/10.1016/j.jep.2016.01.018.
[41] Wang R, Dong Z, Lan X, Liao Z, Chen M. Sweroside alleviated LPS-induced inflammation via SIRT1 mediating NF-kappaB and FOXO1 signaling pathways in RAW264.7 cells. Molecules 2019;24. https://doi.org/10.3390/molecules24050872.
[42] Hsu HY, Wen MH. Lipopolysaccharide-mediated reactive oxygen species and signal transduction in the regulation of interleukin-1 gene expression. J Biol Chem 2002;277:22131–9. https://doi.org/10.1074/jbc.M111883200.
[43] Kraaij MD, van der Kooij SW, Reinders ME, Koekkoek K, Rabelink TJ, van Kooten C, et al. Dexamethasone increases ROS production and T cell suppressive capacity by anti-inflammatory macrophages. Mol Immunol 2011;49:549–57. https://doi.org/10.1016/j.molimm.2011.10.002.
[44] Liu W, Zhao Z, Na Y, Meng C, Wang J, Bai R. Dexamethasone-induced production of reactive oxygen species promotes apoptosis via endoplasmic reticulum stress and autophagy in MC3T3-E1 cells. Int J Mol Med 2018;41:2028–36. https://doi.org/10.3892/ijmm.2018.3412.
[45] Deng S, Dai G, Chen S, Nie Z, Zhou J, Fang H, et al. Dexamethasone induces osteoblast apoptosis through ROS-PI3K/AKT/GSK3beta signaling pathway. Biomed Pharmacother 2019;110:602–8. https://doi.org/10.1016/j.biopha.2018.11.103.
[46] Yao YD, Shen XY, Machado J, Luo JF, Dai Y, Lio CK, et al. Nardochinoid B inhibited the activation of RAW264.7 macrophages stimulated by lipopolysaccharide through activating the Nrf2/HO-1 pathway. Molecules 2019;24. https://doi.org/10.3390/molecules24132482.